AGU ADVANCING EARTH AND SPACE SCIENCES

Geophysical Research Letters®

RESEARCH LETTER
10.1029/2025GL119095

Atmospheric Water Vapor and Precipitation Coupling in Southwestern South America

Raúl Valenzuela[1,2], **Jorge Jara**[3], **and Cristian Martinez-Villalobos**[4,5]

[1]Universidad de O'Higgins (UOH), Instituto de Cs. de la Ingeniería, Rancagua, Chile, [2]Centro de Cs. del Clima y la Resiliencia (CR2), U. de Chile, Santiago, Chile, [3]GFZ Helmholtz Centre for Geosciences, Potsdam, Germany, [4]Faculty of Engineering and Science, Universidad Adolfo Ibañez, Santiago, Chile, [5]Data Observatory Foundation, ANID Technology Center, Santiago, Chile

Key Points:

- First long-term analysis of GNSS-derived water vapor coupled with precipitation across a climatic gradient in Southwestern South America
- Variety of PWV-precipitation coupling at annual, monthly and daily scales as function of latitude
- We suggest a logistic PWV-precipitation relationship for extra-tropics, instead of the classical power law observed in the tropics

Supporting Information:

Supporting Information may be found in the online version of this article.

Correspondence to:

R. Valenzuela,
raul.valenzuela@uoh.cl

Citation:

Valenzuela, R., Jara, J., & Martinez-Villalobos, C. (2025). Atmospheric water vapor and precipitation coupling in southwestern South America. *Geophysical Research Letters*, *52*, e2025GL119095. https://doi.org/10.1029/2025GL119095

Received 28 AUG 2025
Accepted 25 NOV 2025

Author Contributions:

Conceptualization: Raúl Valenzuela, Jorge Jara
Data curation: Raúl Valenzuela
Formal analysis: Raúl Valenzuela, Jorge Jara, Cristian Martinez-Villalobos
Funding acquisition: Raúl Valenzuela
Investigation: Raúl Valenzuela
Methodology: Raúl Valenzuela, Jorge Jara, Cristian Martinez-Villalobos
Project administration: Raúl Valenzuela
Resources: Raúl Valenzuela
Software: Raúl Valenzuela
Supervision: Raúl Valenzuela
Validation: Raúl Valenzuela
Visualization: Raúl Valenzuela, Jorge Jara

Abstract

Most studies linking atmospheric water vapor and precipitation emphasize short records, tropical regions, or the Northern Hemisphere. Long-term variability of water vapor and its coupling with precipitation remain poorly understood across strong latitudinal and climatic gradients. Here we analyze 15–27 years of precipitable water vapor (PWV) from Global Navigation Satellite Systems (GNSS) and co-located rain gauges across southwestern South America. The strength of PWV–precipitation coupling varies systematically with latitude and precipitation regime: high-elevation convective regions show strong coupling across timescales, while extratropical areas dominated by stratiform precipitation exhibit weaker annual and monthly but moderate daily relationships. Seasonal PWV ranges from ∼40 mm in the tropics to ∼6 mm in subpolar regions, yet precipitation varies inversely. Probability distributions reveal a power-law PWV–precipitation relationship only in the tropical Andes, whereas extratropical regions follow a logistic form shaped by positively skewed PWV.

Plain Language Summary

Precipitation depends on the presence of water vapor in the atmosphere, but the connection between them is not the same everywhere. Most previous studies have looked at short time periods or focused on the tropics and the Northern Hemisphere. In this study, we use more than 15 years of water vapor data from Global Navigation Satellite Systems (GNSS) stations in the Southern Hemisphere, specifically across Chile, combined with rain gauge measurements. This region spans 4,000 km, covering very different climates and landscapes. We find that in the mountains of northern and central Chile, precipitation usually occurs when the air suddenly contains much more water vapor. In contrast, in the southern part of the country, precipitation occurs even when the air does not contain very high amounts of water vapor. These results show how the role of water vapor changes with climate and topography, and they provide new observations to test and improve climate models in this region.

1. Introduction

Understanding where and when atmospheric water vapor becomes precipitation remains a key challenge, especially in regions with strong topographic and climatic gradients. While many studies explore the water-vapor–precipitation link using microwave satellite data (e.g., Bretherton et al., 2004), radiosondes (e.g., Holloway & Neelin, 2009), or reanalysis products (e.g., Arraut & Satyamurty, 2009), fewer rely on Global Navigation Satellite Systems (GNSS), which provide Zenith Total Delay (ZTD) data convertible into precipitable water vapor (PWV).

In contrast to reanalyses such as ERA5, which depend on model physics and have coarse resolution, GNSS delivers in situ PWV with high temporal sampling, from daily to sub-second frequencies, enabling the monitoring of both long-term variability and rapid atmospheric processes relevant for weather prediction (Y. Bock & Melgar, 2016). Although the technique has been established for over three decades (Bevis et al., 1992, 1994; Businger et al., 1996), its use in climate research has expanded only recently with improved geodetic precision and long-term data availability (O. Bock et al., 2007; Jin et al., 2007; Santos et al., 2023; Van Malderen et al., 2022).

Most GNSS-PWV studies emphasize the Northern Hemisphere (Maciejewska, 2025; Vaquero-Martínez & Antón, 2021), leaving South America underrepresented. Efforts in Argentina (Calori et al., 2016; Camisay et al., 2020; Fernández et al., 2009), Brazil (Adams et al., 2015), and eastern South America (Aragón Paz et al., 2023) are largely regional or short-term, with Bianchi et al. (2016) providing a rare continental-scale

Writing – original draft:
Raúl Valenzuela, Jorge Jara
Writing – review & editing:
Raúl Valenzuela, Jorge Jara,
Cristian Martinez-Villalobos

analysis. Yet, explicit long-term PWV–precipitation studies remain limited to eastern South America (Campos et al., 2023; Sapucci et al., 2019).

Southwestern South America, particularly Chile, offers a natural laboratory for studying PWV–precipitation coupling across climates and elevations. Its latitudinal extent (17.6°S–55.8°S), sharp climatic gradients, and complex orography yield strong moisture contrasts from the Atacama Desert to Patagonian storm tracks (Garreaud et al., 2009; Vásquez et al., 2025). However, GNSS-based PWV analyses remain scarce, with most relying on reanalysis or short-term data (Falvey & Garreaud, 2005, 2007; Viale et al., 2018; R. A. Valenzuela & Garreaud, 2019).

In the tropics, precipitation typically increases nonlinearly with PWV, approximately as a power law, with a sharp pickup above a critical humidity threshold (Bretherton et al., 2004; Fuchs & Raymond, 2002; Kuo et al., 2017; Neelin et al., 2009, 2022; Peters & Neelin, 2006). This transition reflects the sensitivity of entraining plumes to lower-tropospheric moisture (Ahmed & Neelin, 2018; Kuo et al., 2017) and serves as a diagnostic for convective behavior (Kuo et al., 2018). Whether this functional form extends beyond the tropics, where precipitation is organized by synoptic dynamics and orography, remains uncertain (Ahmed & Neelin, 2018).

Here we test whether a single functional form can describe PWV–precipitation coupling across Chile's diverse climates and elevations. Using 15–27 years of GNSS-PWV data from 14 stations, combined with ERA5 and in situ precipitation, we quantify PWV gradients, validate GNSS retrievals against radiosondes, and evaluate PWV–precipitation relationships across timescales. We further apply a first-passage-time framework to examine how convective and stratiform regimes respond to water vapor availability and whether the tropical power-law paradigm holds in extratropical environments.

2. Data and Methods

2.1. Zenith Total Delay Observations

We used Zenith Total Delay (ZTD) time series from the Nevada Geodetic Laboratory (NGL) database, derived from daily GipsyX 1.0 solutions in the IGS14 reference frame with 5-min sampling and a 7° elevation cutoff (Blewitt et al., 2018). GNSS stations across Chile and adjacent regions with at least 15 years of continuous observations were selected (Figure S1, Table S1 in Supporting Information S1), and all available ZTD data were included. Daily mean ZTD series were visually inspected to detect discontinuities or anomalies. To evaluate sensitivity to outliers, we repeated the analysis after capping values exceeding three standard deviations from the mean day-of-year (DOY) climatology for each station. Results from the capped and full data sets were consistent, indicating negligible influence of outliers.

Although NGL provides operational PWV estimates, these omit vertical temperature corrections between the input meteorological data and station elevation, occasionally producing negative PWV values under dry conditions (Yuan et al., 2023). We therefore derived PWV directly from NGL's ZTD data.

2.2. ERA5-Derived Temperature and Pressure

Converting ZTD into PWV requires surface pressure and 2-m air temperature. Since none of the selected GNSS stations have long-term meteorological records covering the GNSS observational period, we extract these variables from the ERA5 reanalysis (Hersbach et al., 2020), distributed by the Copernicus Climate Data Store (CDS). ERA5 provides hourly fields at 0.25° × 0.25° resolution. For each GNSS site, 2-m temperature and mean sea-level pressure (MSLP) are interpolated from the four nearest grid points using bilinear interpolation. MSLP is then vertically extrapolated to the station altitude using the hypsometric equation:

$$p_2 = p_1 e^{Z/H} \tag{1}$$

where p_2 is the pressure at the GNSS level, p_1 is MSLP (Pa), Z is the GNSS geometric altitude and H the atmospheric scale height (8,000 m, Wallace and Hobbs (2006)).

2.3. GNSS-Based Estimation of Precipitable Water Vapor

ZTD is converted to PWV using standard relationships introduced in GNSS meteorology studies (Bevis et al., 1992, 1994; Businger et al., 1996). The ZTD comprises two components: the Zenith Hydrostatic Delay (ZHD), which is primarily due to the dry atmospheric mass, and the Zenith Wet Delay (ZWD), which arises from the presence of atmospheric water vapor. ZHD is a variable that depends on surface pressure, latitude and geopotential height. Then, ZWD is computed as the difference between ZTD and ZHD. PWV is obtained multiplying ZWD by a temperature dependent factor. To match the temporal resolution of ERA5 data, the 5-min ZTD time series are aggregated to hourly intervals using the mean value. The set of equations used in the study are presented in Text S1 in Supporting Information S1.

2.4. Rain Gauges and Radiosonde Observations

We use daily, quality-controlled precipitation data from two Chilean operational networks: the Dirección General de Aguas (DGA) and the Dirección Meteorológica de Chile (DMC). Combining both networks provides broad spatial coverage across Chile and minimizes the distance between GNSS stations and the nearest rain gauge. Although both agencies apply internal quality controls, we conducted an additional screening to detect anomalous precipitation outside the local rainy season. Suspect values were verified against neighboring stations and synoptic conditions; values associated with identifiable systems (e.g., atmospheric rivers or convection) were retained, while others were flagged as missing. For instance, precipitation events in the Atacama Desert were confirmed via MODIS Terra true-color imagery from NASA Worldview. Because most anomalies corresponded to valid meteorological events, all observations were ultimately preserved.

GNSS-derived PWV estimates were validated against independent radiosonde observations from the Integrated Global Radiosonde Archive (IGRA), version 2.2 (Durre et al., 2018), which includes profiles from the Chilean network operated by the DMC. Radiosonde sites nearest to GNSS stations were used for comparison: ANTF (near JRGN), STDO (near SANT), and PTAR (near PARC). Data were available at 12:00 UTC for ANTF and PTAR, and at 00:00 and 12:00 UTC for STDO. The locations of all rain gauges and radiosonde stations are shown in Figure S1 in Supporting Information S1 and listed in Table S1 in Supporting Information S1.

2.5. Detection of Significant PWV Peaks Using Topographic Prominence

We identify significant peaks in GNSS-derived PWV time series using topographic prominence (TP), a concept from geomorphology that measures a peak's height relative to its surroundings (Dumitrescu & Diac, 2024; Kirmse & De Ferranti, 2017; Torres et al., 2019). While traditionally applied to 2D elevation data, we adapt TP for 1D time series to isolate climatically relevant PWV peaks.

The algorithm identifies local maxima and searches left and right until a higher peak or a fixed window limit is reached. The lowest values within these intervals define the peak's base, and TP is calculated as the difference between the peak and its base.

This method allows selection of significant peaks using a user-defined TP threshold, with values in the same units as PWV (mm), enabling intuitive tuning and effective identification of hydrometeorologically relevant events.

3. Results and Discussion

3.1. GNSS-PWV Estimation and Validation

Selected GNSS stations from NGL span a wide range of Köppen–Geiger climate zones, from hot tropical desert in the north to temperate and polar tundra in the south, enabling climatological analysis across diverse atmospheric conditions (Figure S1 in Supporting Information S1).

We validated GNSS-PWV against radiosonde-derived PWV from nearby launch sites, integrating profiles up to 500 hPa (Figure S2 in Supporting Information S1). Agreement is generally strong, particularly at JRGN–ANTF ($r = 0.97$; slope = 0.94; bias = 0.18 mm; RMSE = 1.56 mm) and PARC–PTAR ($r = 0.92$; slope = 0.83; bias = 0.43 mm; RMSE = 1.94 mm). At SANT–STDO, correspondence is weaker ($r = 0.74$; slope = 0.75; bias = 1.63 mm; RMSE = 3.97 mm), likely due to the ∼100 km horizontal separation and ∼700 m altitude difference.

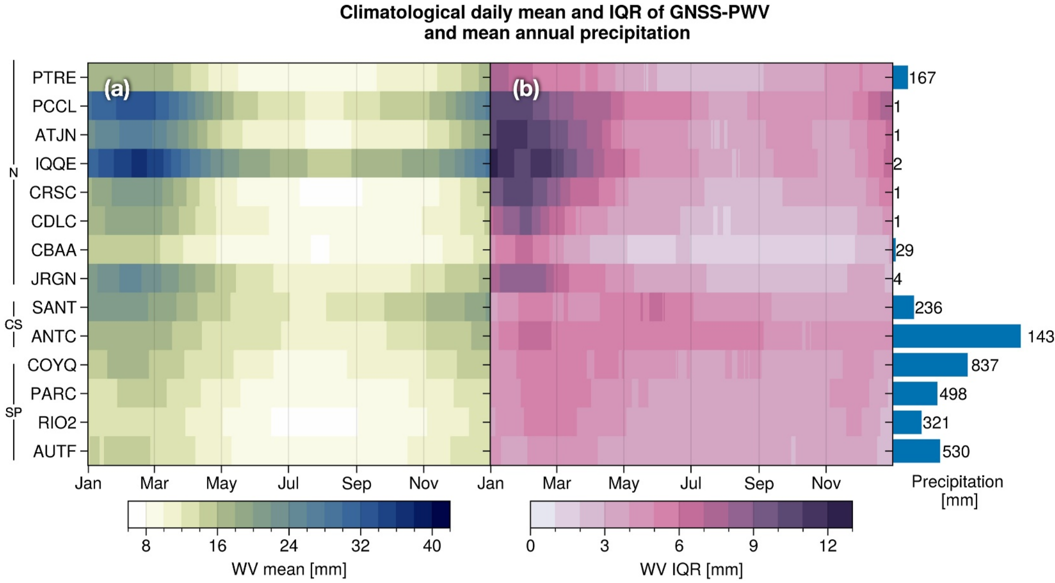

Figure 1. Annual cycle of GNSS-PWV and mean precipitation. (a): Climatological daily PWV by day of year for each station. (b): PWV IQR, indicating intra-annual variability. Stations are ordered north–south and grouped into northern (N), central-southern (CS), and southern Patagonian (SP). Bars in panel (b) show mean annual precipitation from rain gauges. Record lengths are listed in Table S1 in Supporting Information S1.

Despite these local variations, GNSS-PWV reliably captures large-scale temporal moisture variability, supporting its use for long-term climatological analysis. Localized uncertainties from ERA5 inputs or station mismatches appear secondary to the dominant seasonal and latitudinal gradients observed.

3.2. GNSS-PWV Annual Cycle Variability

Climatological daily PWV means were computed by averaging each day of year (DOY) across all years per station. To suppress high-frequency variability, a 90-day, second-order Savitzky–Golay filter (Savitzky & Golay, 1964) was applied, and the interquartile range (IQR) from DOY quartiles was similarly smoothed.

Figure 1 shows the annual PWV cycle, its IQR, and mean annual precipitation, with stations grouped into northern (N), central-southern (CS), and southern Patagonian (SP) clusters. PWV generally peaks in austral summer and reaches a winter minimum, but magnitudes and variability differ regionally. In the north, summer maxima reach ~40 mm at PCCL and IQQE despite >1,100 m elevation difference, declining to ~12 mm in winter. Higher-altitude PTRE and ATJN peak at 18–24 mm with smoother transitions, while CBAA (3,515 m) reaches only 10 mm, highlighting vertical PWV gradients. CS stations (SANT, ANTC) peak at 16–20 mm, with gradual seasonality, and SP sites (COYQ, PARC, RIO2, AUTF) reach 12–18 mm in summer, stabilizing at 6–8 mm in winter. Overall, summer maxima decline poleward, while winter minima remain nearly constant.

PWV variability (IQR) mirrors these patterns. Northern sites reach 12–15 mm in January–February, largely elevation-independent, except PTRE (3,608 m) which is lower. Southward, IQR decreases to 3–6 mm in winter, with SANT showing a May–June peak (6 mm). In contrast, annual precipitation rises sharply from the arid north (<50 mm) to the wet CS (>1,400 mm at ANTC) and declines in SP, reflecting a shift from infrequent and localized convective processes in the northern Andes to broader synoptic, cyclone-driven precipitation south of ~33°S (Falvey & Garreaud, 2005; Garreaud et al., 2009).

3.3. GNSS-PWV Monthly Distribution

We analyze monthly PWV distributions at each GNSS station, fitting log-normal curves to assess shape and variability, following global studies of PWV seasonality (Foster et al., 2006). This allows evaluation of intra-annual PWV evolution across climatic regions and its alignment with local precipitation regimes, which vary strongly with latitude and elevation (Aceituno et al., 2021).

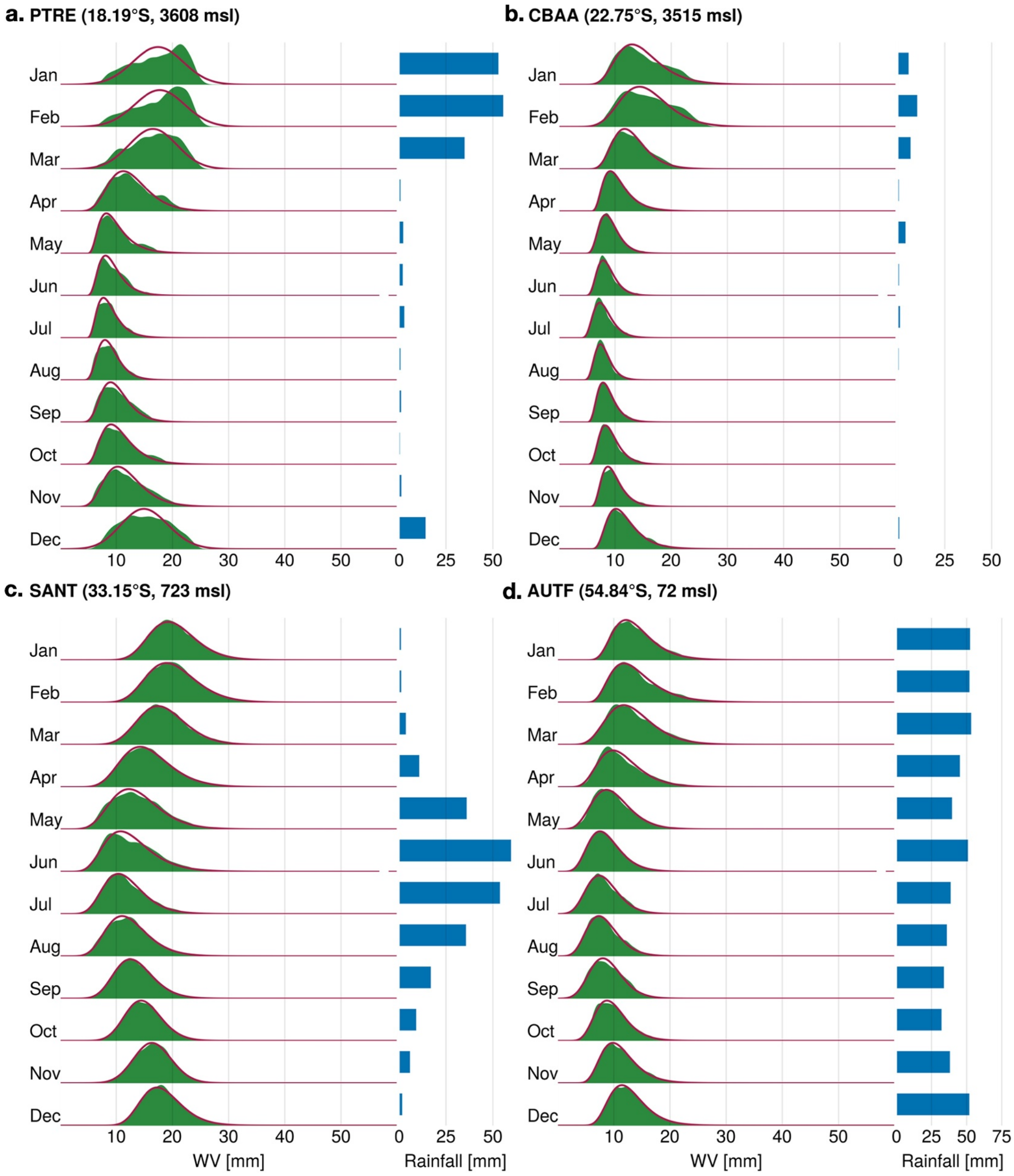

Figure 2. Monthly PWV and precipitation at four GNSS stations across latitudes/elevations: PTRE (18.19°S, 3,608 m), CBAA (22.75°S, 3,515 m), SANT (33.15°S, 723 m), and AUTF (54.84°S, 72 m). Green shading shows PWV KDE, red line a log-normal fit, and adjacent bars mean monthly precipitation from nearby gauges (Table S1 in Supporting Information S1).

Four representative stations illustrate the latitudinal contrasts (Figure 2). At PTRE (18.19°S, 3,608 m), PWV narrows from January to July as modal values fall from 23 to 8 mm, tracking the precipitation regime (30–55 mm January–March, nearly absent April–October). Distributions shift from negative skew (January–March) to positive (April–November), with poor log-normal fit during the wettest months. CBAA (22.75°S, 3,515 m) also narrows through the year, with modal values declining from 13 to 7 mm, but retains a positive skew and closer log-normal fit. Precipitation also peaks January–March but with different PWV–precipitation coupling.

Other northern stations (PCCL, ATJN, IQQE, CRSC, CDLC, JRGN) resemble CBAA, showing wide summer PWV narrowing into winter, positive skew, and modal transitions, but without comparable precipitation. The contrast between PTRE and CBAA with lowland sites reflects differing controls: convective rain and Amazonian inflow versus subsidence from the South Pacific Subtropical Anticyclone at lowland sites (Aceituno & Garreaud, 2025).

Further south, SANT (33.15°S, 723 m) shows little annual change in PWV distribution, which fits log-normal year-round. Modal values decline modestly (19–11 mm), while precipitation peaks in austral winter (~60 mm). Here, precipitation is mainly driven by Atmospheric Rivers reaching ~30°S (Aceituno et al., 2021; R. A. Valenzuela & Garreaud, 2019; Viale et al., 2018). ANTC (37.34°S, 745 m) shows similar PWV but higher precipitation totals (Figure S3 in Supporting Information S1). In southern Patagonia, AUTF (54.84°S, 72 m) shows stable, log-normal PWV distributions (8–12 mm modal values) and nearly constant precipitation (30–50 mm), with slightly reduced totals from July to November. COYQ, PARC, and RIO2 share this pattern, though COYQ concentrates precipitation in April–August (Figure S3 in Supporting Information S1). Unlike northern and CS sites, SP stations lie within the storm track, receiving persistent precipitation largely from Atmospheric Rivers (Garreaud et al., 2014; Viale et al., 2018).

Overall, monthly PWV distributions reveal latitude- and altitude-dependent PWV and precipitation coupling. In the north, high-elevation sites link summer PWV and precipitation via convective activity, a phenomenon connected to Bolivian High inflow and documented in previous studies (e.g., Aceituno & Garreaud, 2025; Falvey & Garreaud, 2005). Although some infrequent episodes related to the passage of cut-off lows can bring precipitation to coastal areas (e.g., Bozkurt et al., 2016), most of the time precipitation is suppressed here under the strong subsidence produced by the South Pacific Subtropical Anticyclone (e.g., Böhm et al., 2020; Vicencio et al., 2024). Southward, precipitation is less tied to PWV central tendency and more to its upper tail, reflecting synoptic control by extratropical cyclones and Atmospheric Rivers (e.g., Aceituno et al., 2021; R. A. Valenzuela & Garreaud, 2019; Viale et al., 2018). As result, PWV distributions, not just their central tendency, are key to understanding PWV–precipitation links across climates.

3.4. Coupling of PWV and Precipitation at Daily Scale

3.4.1. PWV Peaks and Precipitation

Annual and monthly patterns of PWV–precipitation coupling highlight broad climatic controls, but daily-scale analysis offers finer insight into the mechanisms driving precipitation. While previous studies examine daily or sub-daily relationships between PWV and precipitation primarily in tropical settings (Bretherton et al., 2004; Fuchs & Raymond, 2002; Kuo et al., 2017, 2018; Neelin et al., 2009), our GNSS-PWV records enable us to analyze tropical and extratropical differences.

We quantify this relationship by calculating the conditional probability of precipitation on days when PWV reaches a peak. PWV peaks are identified using the topographic prominence (TP) algorithm applied to daily GNSS-PWV time series. This probability is defined as:

$$P(\text{rain} \mid \text{peak}) = \frac{P(\text{rain} > 0 \cap \text{peak})}{P(\text{peak})} \tag{2}$$

An example of PWV peaks detected using the TP method for SANT during 2011 is shown in Figure 3a. Here, two prominence values are selected: 7 and 10 mm. Lower thresholds (e.g., 7 mm) capture more frequent events, while higher thresholds (e.g., 10 mm) isolate more extreme, less frequent PWV anomalies. These peaks modulate around a seasonal PWV cycle (10–20 mm), highlighting the role of synoptic variability (e.g., sub-weekly scale) in daily moisture fluctuations (Benevides et al., 2015; Liang et al., 2020). Figure 3b shows the resulting conditional probabilities across all stations for four TP thresholds (3, 7, 10, 15 mm). At low-elevation northern stations (PCCL, IQQE, ATJN, CRSC, CDLC, JRGN), conditional probabilities are near zero, consistent with infrequent precipitation. At higher-elevation (>3,000 msl) PTRE and CBAA, conditional probabilities reach up to 0.93 and 0.5, respectively, reflecting stronger PWV–precipitation coupling likely associated with convective events fueled by elevated moisture transport from the Bolivian High (Aceituno & Garreaud, 2025; Aceituno et al., 2021).

In the central-southern group (SANT, ANTC), probabilities range from 0.23 to 0.62. SANT shows a gradual increase with higher TP, while ANTC peaks at intermediate thresholds (7 mm). In southern-patagonian (COYQ, PARC, RIO2, AUTF) probabilities are moderate to high (0.41–0.68) but decreases at the highest thresholds, suggesting that some PWV anomalies are unrelated to daily precipitation. We interpret this behavior as the

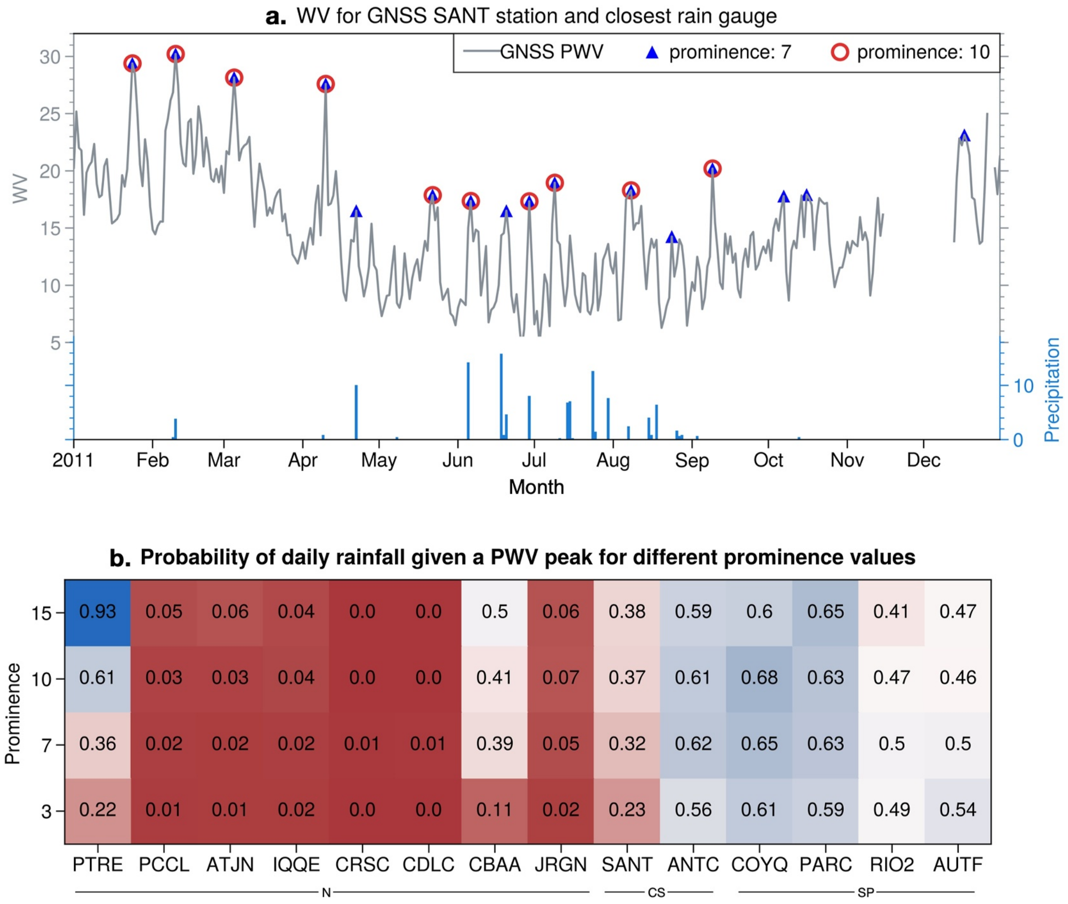

Prominence	PTRE	PCCL	ATJN	IQQE	CRSC	CDLC	CBAA	JRGN	SANT	ANTC	COYQ	PARC	RIO2	AUTF
15	0.93	0.05	0.06	0.04	0.0	0.0	0.5	0.06	0.38	0.59	0.6	0.65	0.41	0.47
10	0.61	0.03	0.03	0.04	0.0	0.0	0.41	0.07	0.37	0.61	0.68	0.63	0.47	0.46
7	0.36	0.02	0.02	0.02	0.01	0.01	0.39	0.05	0.32	0.62	0.65	0.63	0.5	0.5
3	0.22	0.01	0.01	0.02	0.0	0.0	0.11	0.02	0.23	0.56	0.61	0.59	0.49	0.54

Figure 3. (a) PWV peak detection at SANT station in 2011 using topographic prominence. Gray line: GNSS-PWV time series. Blue triangles: peaks with 7 mm threshold; red circles: 10 mm threshold. Blue bars: daily precipitation from nearby Pudahuel gauge. (b) Conditional probability matrix of precipitation on PWV peak days for all stations and four thresholds (3, 7, 10, 15 mm). Stations grouped as northern (N), central-southern (CS), and southern Patagonian (SP). Warmer (cooler) colors show lower (higher) probabilities.

influence of stratiform and post-frontal systems (Garreaud et al., 2014) that efficiently produce precipitation without the need of having a sharp PWV peak.

3.4.2. Coupled PWV and Precipitation Distributions

The relationship between PWV and precipitation has often been studied from a probability distribution perspective, mainly in the tropics, where both theory and observations support a power law dependence (Hottovy & Stechmann, 2015; Neelin et al., 2022; Stechmann & Neelin, 2011, 2014). Here, we test whether this relationship also holds in extratropical regions.

We examine how precipitation varies with PWV magnitude by binning PWV values and computing the median precipitation in each bin. Bins of 6 mm with 3 mm overlap are used to reduce noise between groups. Results for PTRE, CBAA, SANT, and AUTF (Figures 4a–4d) show that PTRE (18.19°S) follows the tropical power law, while other stations depart from it. For instance, CBAA (22.75°S) exhibits higher precipitation at low PWV and lower precipitation at mid PWV compared to the power law fit, SANT (33.15°S) shows the opposite pattern, and AUTF (54.84°S) resembles CBAA. Similar deviations are observed at other sites that have precipitation at extratropical latitudes (Figure S5 in Supporting Information S1).

These results suggest that a power law is appropriate only for PTRE, consistent with its tropical location, convective precipitation, and negatively skewed PWV distribution during the wet season (e.g., Peters & Neelin, 2006). In contrast, extratropical sites align better with a logistic form, characterized by slow precipitation

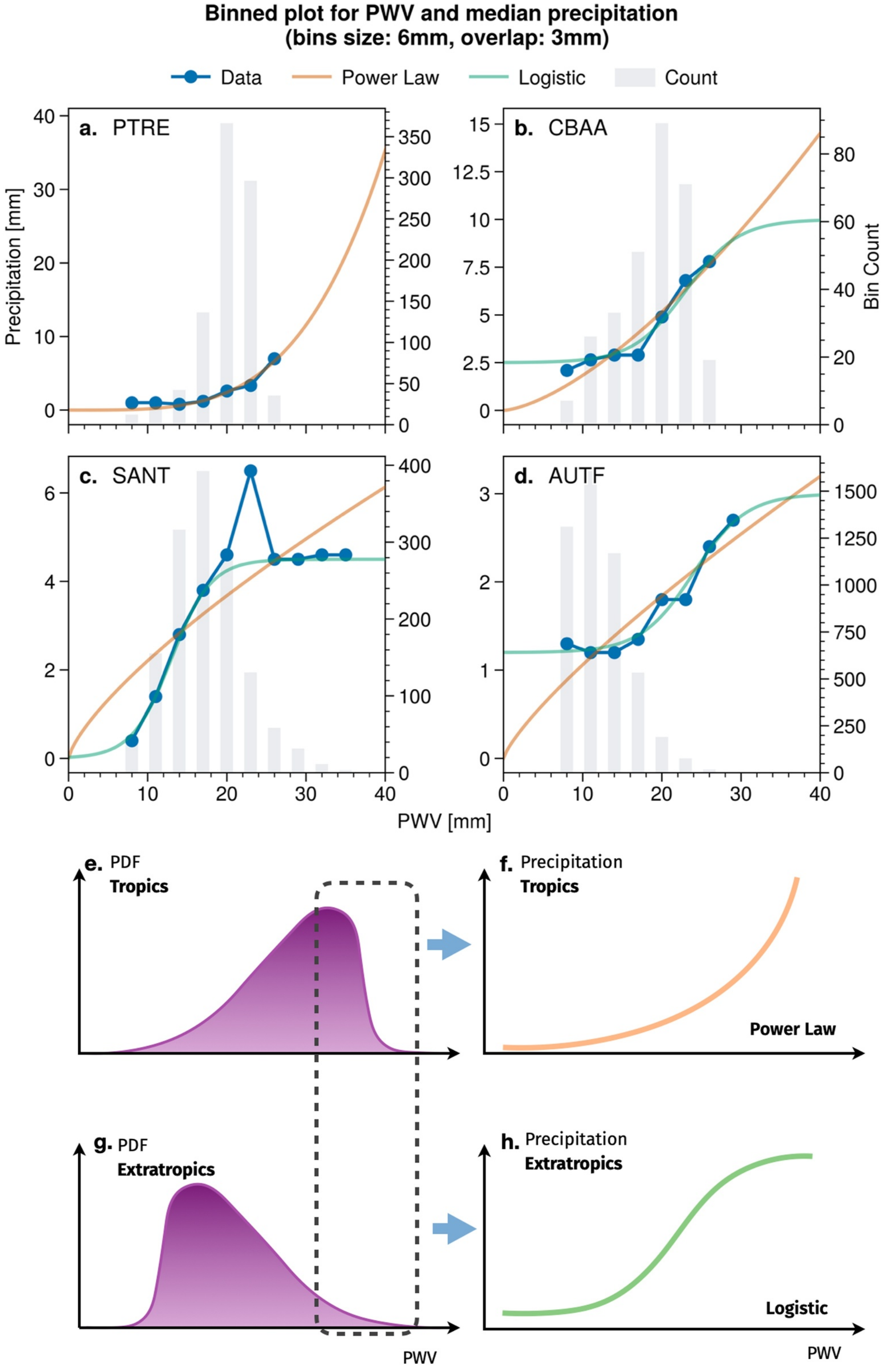

Figure 4. (a–d) Median precipitation versus binned PWV. Bins: 6 mm wide, 3 mm overlap. Empirical PWV–precipitation (blue points) compared with two models: power law (orange) and logistic (green). Bin counts shown as gray bars. (e–h) Conceptual model linking PWV distribution to PWV–precipitation using SN14: hypothetical PWV with negative (e) and positive (g) skew, and PWV–precipitation following power law (f) or logistic (h). Dashed box marks the upper tail of tropical/extratropical PWV distribution.

increases at low PWV, rapid rises at intermediate values, and saturation or flattening at the upper tail (Figures 4b–4d).

We investigate the PWV-precipitation relationship from a theoretical standpoint to elucidate what factors can contribute to a departure from the well-documented power law relationship in favor of a logistic relationship. Since our previous result shows a coupling between PWV peaks and precipitation, and considering the stochastic behavior of PWV (e.g., Figure 3a), a model that includes precipitation triggering based on a PWV thresholds seems adequate. For this analysis, we use a first-passage-time model proposed by Stechmann and Neelin (2014), hereafter SN14. A first-passage-time model is a stochastic model that aims to reproduce stochastic processes triggered by first-passage events. In other words, these are processes involving events triggered when a given threshold is reached. As such, SN14 assumes that PWV has a stochastic behavior and that precipitation is triggered or suppressed when PWV crosses a given threshold. In the SN14 study, a three-state model is proposed, which includes triggers for convective and stratiform precipitation and has the following stochastic functions:

$$\frac{dq}{dt} = E + D_{np}\epsilon \qquad \text{until} \qquad q = q_c \tag{3}$$

$$\frac{dq}{dt} = -P_c + D_c\epsilon \qquad \text{until} \qquad q = q_s \tag{4}$$

$$\frac{dq}{dt} = -P_s + D_s\epsilon \qquad \text{until} \qquad q = q_{np} \quad \text{or} \quad q_c \tag{5}$$

where q is PWV, t is time, E is a mean moisture source (e.g., surface fluxes and moisture advection), D_{np}, D_c, and D_s are the variances of water vapor forcing for non-precipitating, convective, and stratiform states, P_c and P_s are the corresponding precipitation rates, and ϵ is Gaussian white noise.

We implemented SN14 using an Euler–Maruyama solver, updating the new q values as:

$$\Delta q = B * \Delta t + \sqrt{D^2 * \Delta t} * \epsilon, \tag{6}$$

where B corresponds to E, P_c, or P_s depending on the state, and D^2 corresponds to D_{np}, D_c, or D_s for non-precipitating, convective, or stratiform conditions, respectively.

We explore a parameter space slightly modified from SN14 (Table S2 in Supporting Information S1) to reproduce the PWV magnitudes observed in our GNSS time series (Figure 2 and Figure S3 in Supporting Information S1). Relative to the original study, we reduce P_c, increase P_s, set E drier, decrease D_c^2, increase D_{np}^2, and vary D_s^2 both below and above the SN14 values. All PWV thresholds are lowered to match observed ranges.

The full parameter set gives 170,100 combinations, each run for 1,000 iterations with a time step of 0.01 hr. For each run we compute mean precipitation per overlapping PWV bin, retain simulations producing precipitation up to the last PWV bin of 40 mm, and fit both power law and logistic functions. We then compare R^2 values over 10,000 random subsets of simulations. Logistic fits consistently outperform power laws, indicating that the extratropical PWV–precipitation relationship is more likely logistic (Figure S6 in Supporting Information S1).

With this result, we propose that the PWV-precipitation relationship in the extratropics differs from the tropical relationship as represented in the schematics of Figures 4e–4h. The extratropics have a positive skewed PWV distribution, meaning that the upper tail of the PWV distribution is a strong limiting factor for producing precipitation. In addition, the non precipitating forcing is larger and can condition the precipitation triggering at mid PWV values. Lastly, when convective and stratiform precipitation rates are close to each other and the stratiform forcing is larger than the convective forcing, more continuous precipitation episodes emerge, also influencing the flattening of precipitation in the upper tail of PWV distribution.

Unexplained features remain, such as the overshooting peak observed in SANT (Figure 4c), ANTC, COYQ, PARC, and RIO2 (Figure S5 in Supporting Information S1), which we cannot reproduce with the SN14 model. A cursory examination of results in SANT suggests that a potential mechanism related to the overshooting peak is the impact of transient Atmospheric Rivers associated with heavy daily precipitation (Figure S7 in Supporting Information S1, R. A. Valenzuela & Garreaud, 2019; Viale et al., 2018). Another feature is the sharp drop in precipitation at the highest PWV in COYQ, PARC, and RIO2 (Figure S5 in Supporting Information S1). This feature might reflect sampling limitations (e.g., unfrequent cases) or additional processes not captured by the SN14 model.

4. Conclusions

We analyzed the co-variability of precipitable water vapor (PWV) and precipitation across Chile's full latitudinal and climatic range, using 15–27 years of GNSS-derived PWV combined with reanalysis and in situ precipitation. This integrated approach reveals how moisture availability translates into precipitation from the tropics to the extratropics.

The annual PWV cycle peaks in arid northern Chile and weakens southward. In the north, elevated summer PWV at low elevations reflects coastal moisture transport from the equator (Vicencio et al., 2024), yet precipitation remains scarce due to subsidence from the South Pacific Subtropical Anticyclone. At higher Andean sites, lower PWV coexists with convective precipitation linked to episodic Amazonian inflow and Bolivian High circulation (Falvey & Garreaud, 2005; Minvielle & Garreaud, 2011). In central-southern Chile, precipitation occurs mainly in austral winter when PWV is low, indicating that precipitation depends on the upper tail of its positively skewed distribution. In Patagonia, weak PWV seasonality and persistent storms produce year-round precipitation with a stochastic, transport-driven coupling, largely modulated by Atmospheric Rivers.

Daily-scale analysis shows PWV peaks coincide with convective precipitation at high-altitude northern sites, while coupling weakens southward under stratiform and post-frontal regimes. The tropical PWV–precipitation power law applies only at high-altitude PTRE; extratropical stations follow a logistic relationship. A first-passage-time model attributes this contrast to PWV skewness: negatively skewed tropical PWV favors power-law growth, whereas positive skewness in extratropical PWV yields a logistic saturation at high values.

Overall, PWV–precipitation coupling in Chile varies systematically with climate and elevation, offering an observational baseline for climate model validation. Future work should further address large-scale moisture transport and wind dynamics, particularly Atmospheric Rivers, in shaping the PWV-precipitation relationship across diverse environments. Additionally, exploration of rapid PWV variations at sub-daily scale should be performed to further understand PWV-precipitation relationship at meteorological relevant scales.

Conflict of Interest

The authors declare no conflicts of interest relevant to this study.

Data Availability Statement

Zenith Total Delay (ZTD) time series are provided by the Nevada Geodetic Laboratory (2025). Surface pressure and 2-m temperature data are obtained from the ERA5 reanalysis distributed by the Copernicus Climate Data Store (2025). Daily precipitation records from Dirección General de Aguas (DGA) and Dirección Meteorológica de Chile (DMC) collected by the Center for Climate and Resilience Research (2025). Radiosonde profiles are provided by the National Centers for Environmental Information (2025). The topographic prominence code was implemented in Python using OpenAI's GPT-4o mini model and is available at Zenodo (R. Valenzuela, 2025b). The implementation of the SN14 model follows publicly available code retrieved using Claude Sonnet 4 (https://claude.ai/). The code was generated by uploading Stechmann and Neelin (2014) and issuing the prompt "write a python code to implement the three-state model." The retrieved implementation was revised, tested to reproduce the results of the original study, and it is available at Zenodo (R. Valenzuela, 2025a).

Acknowledgments
Bastián Rubio assisted with GNSS and precipitation data analysis. R.V. acknowledges funding from ANID Fondecyt Iniciación Grant 11230184 and partial funding from FONDAP/ANID 1523A0002. J.J. acknowledges partial funding from the Marie Skłodowska-Curie Postdoctoral Fellowship (Grant 101066069) and the Volkswagen Foundation (Grant 0200087-00). C.M.-V. acknowledges support from ANID Fondecyt Iniciación 11250471 and Data Observatory Foundation ANID Technology Center DO210001. We thank the Editor and two anonymous reviewers for their constructive comments, which helped to improve the final version of the manuscript.

References

Aceituno, P., Boisier, J. P., Garreaud, R., Rondanelli, R., & Rutllant, J. A. (2021). Climate and weather in Chile. In B. Fernández & J. Gironás (Eds.), *Water resources of Chile* (Vol. 8, pp. 7–29). Springer International Publishing. (Series Title: World Water Resources). https://doi.org/10.1007/978-3-030-56901-3_2

Aceituno, P., & Garreaud, R. (2025). The climate of the South American Altiplano. In *Oxford research encyclopedia of climate science*. Oxford University Press. https://doi.org/10.1093/acrefore/9780190228620.013.977

Adams, D. K., Fernandes, R. M. S., Holub, K. L., Gutman, S. I., Barbosa, H. M. J., Machado, L. A. T., et al. (2015). The Amazon Dense GNSS meteorological network: A new approach for examining water vapor and deep convection interactions in the tropics. *Bulletin of the American Meteorological Society*, *96*(12), 2151–2165. https://doi.org/10.1175/BAMS-D-13-00171.1

Ahmed, F., & Neelin, J. D. (2018). Reverse engineering the tropical precipitation–buoyancy relationship. *Journal of the Atmospheric Sciences*, *75*(5), 1587–1608. https://doi.org/10.1175/JAS-D-17-0333.1

Aragón Paz, J. M., Mendoza, L. P. O., & Fernández, L. I. (2023). Near-real-time GNSS tropospheric IWV monitoring system for South America. *GPS Solutions*, *27*(2), 93. https://doi.org/10.1007/s10291-023-01436-2

Arraut, J. M., & Satyamurty, P. (2009). Precipitation and water vapor transport in the Southern Hemisphere with emphasis on the South American Region. *Journal of Applied Meteorology and Climatology*, *48*(9), 1902–1912. (Publisher: American Meteorological Society). https://doi.org/10.1175/2009jamc2030.1

Benevides, P., Catalao, J., & Miranda, P. M. A. (2015). On the inclusion of GPS precipitable water vapour in the nowcasting of rainfall. *Natural Hazards and Earth System Sciences*, *15*(12), 2605–2616. https://doi.org/10.5194/nhess-15-2605-2015

Bevis, M., Businger, S., Chiswell, S., Herring, T. A., Anthes, R. A., Rocken, C., & Ware, R. H. (1994). GPS meteorology: Mapping zenith wet delays onto precipitable water. *Journal of Applied Meteorology*, *33*(3), 379–386. https://doi.org/10.1175/1520-0450(1994)033⟨0379:GMMZWD⟩2.0.CO;2

Bevis, M., Businger, S., Herring, T. A., Rocken, C., Anthes, R. A., & Ware, R. H. (1992). GPS meteorology: Remote sensing of atmospheric water vapor using the global positioning system. *Journal of Geophysical Research*, *97*(D14), 15787–15801. https://doi.org/10.1029/92JD01517

Bianchi, C. E., Mendoza, L. P. O., Fernández, L. I., Natali, M. P., Meza, A. M., & Moirano, J. F. (2016). Multi-year GNSS monitoring of atmospheric IWV over Central and South America for climate studies. *Annales Geophysicae*, *34*(7), 623–639. (Publisher: Copernicus GmbH). https://doi.org/10.5194/angeo-34-623-2016

Blewitt, G., Hammond, W., & Kreemer, C. (2018). Harnessing the GPS data explosion for interdisciplinary science. *Eos*, *99*. https://doi.org/10.1029/2018EO104623

Bock, O., Guichard, F., Janicot, S., Lafore, J. P., Bouin, M., & Sultan, B. (2007). Multiscale analysis of precipitable water vapor over Africa from GPS data and ECMWF analyses. *Geophysical Research Letters*, *34*(9). (Publisher: American Geophysical Union (AGU)). https://doi.org/10.1029/2006gl028039

Bock, Y., & Melgar, D. (2016). Physical applications of GPS geodesy: A review. *Reports on Progress in Physics*, *79*(10), 106801. https://doi.org/10.1088/0034-4885/79/10/106801

Böhm, C., Reyers, M., Schween, J. H., & Crewell, S. (2020). Water vapor variability in the Atacama Desert during the 20th century. *Global and Planetary Change*, *190*, 103192. https://doi.org/10.1016/j.gloplacha.2020.103192

Bozkurt, D., Rondanelli, R., Garreaud, R., & Arriagada, A. (2016). Impact of warmer eastern tropical Pacific SST on the March 2015 Atacama Floods. *Monthly Weather Review*, *144*(11), 4441–4460. https://doi.org/10.1175/MWR-D-16-0041.1

Bretherton, C. S., Peters, M. E., & Back, L. E. (2004). Relationships between water vapor path and precipitation over the tropical oceans. *Journal of Climate*, *17*(7), 1517–1528. (Publisher: American Meteorological Society). https://doi.org/10.1175/1520-0442(2004)017⟨1517:rbwvpa⟩2.0.co;2

Businger, S., Chiswell, S. R., Bevis, M., Duan, J., Anthes, R. A., Rocken, C., et al. (1996). The promise of GPS in atmospheric monitoring. *Bulletin of the American Meteorological Society*, *77*(1), 5–18. https://doi.org/10.1175/1520-0477(1996)077⟨0005:TPOGIA⟩2.0.CO;2

Calori, A., Santos, J., Blanco, M., Pessano, H., Llamedo, P., Alexander, P., & De La Torre, A. (2016). Ground-based GNSS network and integrated water vapor mapping during the development of severe storms at the Cuyo region (Argentina). *Atmospheric Research*, *176–177*, 267–275. https://doi.org/10.1016/j.atmosres.2016.03.002

Camisay, M., Rivera, J., Mateo, M., Morichetti, P., & Mackern, M. (2020). Estimation of integrated water vapor derived from Global Navigation Satellite System observations over Central-Western Argentina (2015–2018). Validation and usefulness for the understanding of regional precipitation events. *Journal of Atmospheric and Solar-Terrestrial Physics*, *197*, 105143. https://doi.org/10.1016/j.jastp.2019.105143

Campos, T. B., Sapucci, L. F., Eichholz, C., Machado, L. A. T., & Adams, D. K. (2023). The sensitivity of GPS precipitable water vapor jumps to intense precipitation associated with tropical organized convective systems. *Atmosphere*, *14*(2), 262. https://doi.org/10.3390/atmos14020262

Center for Climate and Resilience Research. (2025). CR2 daily precipitation ending 2023 [Dataset]. *Zenodo*. https://doi.org/10.5281/zenodo.16989768

Copernicus Climate Data Store. (2025). ERA5 reanalysis [Dataset]. Retrieved from https://cds.climate.copernicus.eu/datasets/reanalysis-era5-single-levels?tab=download

Dumitrescu, G. A., & Diac, P. F. (2024). An efficient algorithm for computing mountain prominence in almost linear time. In *2024 International Conference on INnovations in Intelligent SysTems and Applications (INISTA)* (pp. 1–6). IEEE. https://doi.org/10.1109/INISTA62901.2024.10683840

Durre, I., Yin, X., Vose, R. S., Applequist, S., & Arnfield, J. (2018). Enhancing the data coverage in the integrated global radiosonde archive. *Journal of Atmospheric and Oceanic Technology*, *35*(9), 1753–1770. https://doi.org/10.1175/JTECH-D-17-0223.1

Falvey, M., & Garreaud, R. (2007). Wintertime precipitation episodes in Central Chile: Associated meteorological conditions and orographic influences. *Journal of Hydrometeorology*, *8*(2), 171–193. https://doi.org/10.1175/JHM562.1

Falvey, M., & Garreaud, R. D. (2005). Moisture variability over the South American Altiplano during the South American Low Level Jet Experiment (SALLJEX) observing season. *Journal of Geophysical Research*, *110*(D22), D22105. https://doi.org/10.1029/2005JD006152

Fernández, L. I., Meza, A., & Natali, M. P. (2009). Determinación del contenido de vapor de agua precipitable (PWV) a partir de mediciones GPS: Primeros resultados en Argentina. *Geoacta*, *34*(2). (Section: Trabajos científicos).

Foster, J., Bevis, M., & Raymond, W. (2006). Precipitable water and the lognormal distribution. *Journal of Geophysical Research*, *111*(D15), D15102. https://doi.org/10.1029/2005JD006731

Fuchs, Z., & Raymond, D. J. (2002). Large-scale modes of a nonrotating atmosphere with water vapor and cloud–radiation feedbacks. *Journal of the Atmospheric Sciences*, *59*(10), 1669–1679. https://doi.org/10.1175/1520-0469(2002)059⟨1669:LSMOAN⟩2.0.CO;2

Garreaud, R. D., Gabriela Nicora, M., Bürgesser, R. E., & Ávila, E. E. (2014). Lightning in Western Patagonia. *Journal of Geophysical Research: Atmospheres*, *119*(8), 4471–4485. https://doi.org/10.1002/2013JD021160

Garreaud, R. D., Vuille, M., Compagnucci, R., & Marengo, J. (2009). Present-day South American climate. *Palaeogeography, Palaeoclimatology, Palaeoecology*, *281*(3–4), 180–195. https://doi.org/10.1016/j.palaeo.2007.10.032

Hersbach, H., Bell, B., Berrisford, P., Hirahara, S., Horányi, A., Muñoz-Sabater, J., et al. (2020). The ERA5 global reanalysis. *Quarterly Journal of the Royal Meteorological Society*, *146*(730), 1999–2049. https://doi.org/10.1002/qj.3803

Holloway, C. E., & Neelin, J. D. (2009). Moisture vertical structure, column water vapor, and tropical deep convection. *Journal of the Atmospheric Sciences*, *66*(6), 1665–1683. https://doi.org/10.1175/2008jas2806.1

Hottovy, S., & Stechmann, S. N. (2015). Threshold models for rainfall and convection: Deterministic versus stochastic triggers. *SIAM Journal on Applied Mathematics*, *75*(2), 861–884. https://doi.org/10.1137/140980788

Jin, S., Park, J., Cho, J., & Park, P. (2007). Seasonal variability of GPS-derived zenith tropospheric delay (1994–2006) and climate implications. *Journal of Geophysical Research*, *112*(D9), 2006JD007772. https://doi.org/10.1029/2006JD007772

Kirmse, A., & De Ferranti, J. (2017). Calculating the prominence and isolation of every mountain in the world. *Progress in Physical Geography: Earth and Environment*, *41*(6), 788–802. https://doi.org/10.1177/0309133317738163

Kuo, Y.-H., Neelin, J. D., & Mechoso, C. R. (2017). Tropical convective transition statistics and causality in the water vapor–precipitation relation. *Journal of the Atmospheric Sciences*, *74*(3), 915–931. https://doi.org/10.1175/JAS-D-16-0182.1

Kuo, Y.-H., Schiro, K. A., & Neelin, J. D. (2018). Convective transition statistics over tropical oceans for climate model diagnostics: Observational baseline. *Journal of the Atmospheric Sciences*, *75*(5), 1553–1570. https://doi.org/10.1175/JAS-D-17-0287.1

Liang, H., Zhang, Y., Cao, L., & Cao, Y. (2020). Temporal relations between precipitable water vapour and precipitation during wet seasons based on nearly two decades of data from the Lhasa River valley, Tibetan Plateau. *International Journal of Climatology*, *40*(3), 1656–1668. https://doi.org/10.1002/joc.6293

Maciejewska, A. (2025). Use of tropospheric delay in GNSS-Based climate monitoring—A review. *Remote Sensing*, *17*(9), 1501. https://doi.org/10.3390/rs17091501

Minvielle, M., & Garreaud, R. D. (2011). Projecting Rainfall changes over the South American Altiplano. *Journal of Climate*, *24*(17), 4577–4583. https://doi.org/10.1175/JCLI-D-11-00051.1

National Centers for Environmental Information. (2025). Integrated global radiosonde archive [Dataset]. Retrieved from https://www.ncei.noaa.gov/data/integrated-global-radiosonde-archive/access/data-por/

Neelin, J. D., Martinez-Villalobos, C., Stechmann, S. N., Ahmed, F., Chen, G., Norris, J. M., et al. (2022). Precipitation extremes and water vapor: Relationships in current climate and implications for climate change. *Current Climate Change Reports*, *8*(1), 17–33. https://doi.org/10.1007/s40641-021-00177-z

Neelin, J. D., Peters, O., & Hales, K. (2009). The transition to strong convection. *Journal of the Atmospheric Sciences*, *66*(8), 2367–2384. https://doi.org/10.1175/2009JAS2962.1

Nevada Geodetic Laboratory. (2025). The MAGNET GPS network [Dataset]. Retrieved from https://geodesy.unr.edu/magnet/rinex/

Peters, O., & Neelin, J. D. (2006). Critical phenomena in atmospheric precipitation. *Nature Physics*, *2*(6), 393–396. https://doi.org/10.1038/nphys314

Santos, M., Balidakis, K., Klos, A., Pacione, R., & Rees, J. (2023). Long-term ground-based GNSS-derived ZTD trends for climate. In *XXVIII General Assembly of the International Union of Geodesy and Geophysics (IUGG)*. https://doi.org/10.57757/IUGG23-3515

Sapucci, L. F., Machado, L. A. T., De Souza, E. M., & Campos, T. B. (2019). Global positioning system precipitable water vapour (GPS-PWV) jumps before intense rain events: A potential application to nowcasting. *Meteorological Applications*, *26*(1), 49–63. https://doi.org/10.1002/met.1735

Savitzky, A., & Golay, M. J. E. (1964). Smoothing and differentiation of data by simplified least squares procedures. *Analytical Chemistry*, *36*(8), 1627–1639. https://doi.org/10.1021/ac60214a047

Stechmann, S. N., & Neelin, J. D. (2011). A stochastic model for the transition to strong convection. *Journal of the Atmospheric Sciences*, *68*(12), 2955–2970. https://doi.org/10.1175/JAS-D-11-028.1

Stechmann, S. N., & Neelin, J. D. (2014). First-passage-time prototypes for precipitation statistics. *Journal of the Atmospheric Sciences*, *71*(9), 3269–3291. https://doi.org/10.1175/JAS-D-13-0268.1

Torres, R. N., Milani, F., & Fraternali, P. (2019). Algorithms for mountain peaks discovery: A comparison. In *Proceedings of the 34th ACM/SIGAPP Symposium on Applied Computing* (pp. 667–674). Limassol Cyprus: ACM. https://doi.org/10.1145/3297280.3297343

Valenzuela, R. (2025a). Stechman and Neelin 2014 stochastic model [Software]. https://doi.org/10.5281/zenodo.16990113

Valenzuela, R. (2025b). Topographic Prominance for time series [Software]. https://doi.org/10.5281/zenodo.15650684

Valenzuela, R. A., & Garreaud, R. D. (2019). Extreme daily rainfall in Central-Southern Chile and its relationship with low-level horizontal water vapor fluxes. *Journal of Hydrometeorology*, *20*(9), 1829–1850. https://doi.org/10.1175/JHM-D-19-0036.1

Van Malderen, R., Santos, M., & Zhang, K. (2022). Editorial for the special issue “Climate modelling and monitoring using GNSS”. *Remote Sensing*, *14*(17), 4371. (Publisher: MDPI AG). https://doi.org/10.3390/rs14174371

Vaquero-Martínez, J., & Antón, M. (2021). Review on the role of GNSS meteorology in monitoring water vapor for atmospheric physics. *Remote Sensing*, *13*(12), 2287. https://doi.org/10.3390/rs13122287

Vásquez, N. A., Mendoza, P. A., Lagos-Zuñiga, M., Scaff, L., Muñoz-Castro, E., & Vargas, X. (2025). Robust spatial changes in climate classes: Insights from bias-corrected CMIP6 models across Chile. *Environmental Research Letters*, *20*(1), 014061. https://doi.org/10.1088/1748-9326/ad9d5b

Viale, M., Valenzuela, R., Garreaud, R. D., & Ralph, F. M. (2018). Impacts of atmospheric rivers on precipitation in Southern South America. *Journal of Hydrometeorology*, *19*(10), 1671–1687. https://doi.org/10.1175/JHM-D-18-0006.1

Vicencio, J., Böhm, C., Schween, J. H., Löhnert, U., & Crewell, S. (2024). A comparative study of the atmospheric water vapor in the Atacama and Namib Desert. *Global and Planetary Change*, *232*, 104320. https://doi.org/10.1016/j.gloplacha.2023.104320

Wallace, J. M., & Hobbs, P. V. (2006). *Atmospheric science: An introductory survey*. Elsevier. https://doi.org/10.1016/c2009-0-00034-8

Yuan, P., Blewitt, G., Kreemer, C., Hammond, W. C., Argus, D., Yin, X., et al. (2023). An enhanced integrated water vapour dataset from more than 10 000 global ground-based GPS stations in 2020. *Earth System Science Data*, *15*(2), 723–743. https://doi.org/10.5194/essd-15-723-2023